BRPF3 knockdown or inhibition moderately reverses olaparib resistance in high grade serous ovarian carcinoma

Benjamin G. Bitler[1], Tomomi M. Yamamoto[1], Alexandra McMellen[2], Hyunmin Kim[3], and Zachary L. Watson[1#]

[1] Division of Reproductive Sciences, Department of Obstetrics and Gynecology, University of Colorado School of Medicine, Aurora, CO 80045, USA

[2] Cancer Biology Graduate Program, University of Colorado, Aurora, CO 80045, USA

[3] Translational Bioinformatics and Cancer Systems Biology Laboratory, Division of Medical Oncology, Department of Medicine, University of Colorado Anschutz Medical Campus, Aurora, CO 80045, USA

Corresponding Author:

Zachary L. Watson, PhD

Division of Reproductive Sciences

Department of Obstetrics and Gynecology

12700 E. 19th Ave, MS 8613

Aurora, CO 80045

Phone: 303-724-8682

Fax: 303-724-3512

zachary.watson@cuanschutz.edu

Abstract

Background: PARP inhibitors (PARPi) kill cancer cells by stalling DNA replication and preventing DNA repair, resulting in a critical accumulation of DNA damage. Resistance to PARPi is a growing clinical problem in the treatment of high grade serous ovarian carcinoma (HGSOC). Acetylation of histone H3 lysine 14 (H3K14ac) and associated histone acetyltransferases (HATs) have known functions in DNA repair and replication, but their expression and activities have not been examined in the context of PARPi-resistant HGSOC.

Results: Using mass spectrometry profiling of histone modifications, we observed altered H3K14ac enrichment in PARPi-resistant HGSOC cells relative to isogenic PARPi-sensitive lines. By RT-qPCR and RNA-Seq, we also observed altered expression of numerous HATs in PARPi-resistant HGSOC cells and a PARPi-resistant PDX model. Knockdown of HATs only modestly altered PARPi response, although knockdown and inhibition of PCAF significantly increased resistance. Pharmacologic inhibition of HBO1 severely depleted H3K14ac but did not affect PARPi response. However, knockdown and inhibition of BRPF3, which is known to interact in a complex with HBO1, did reduce PARPi resistance.

Conclusions: This study demonstrates that severe depletion of H3K14ac does not affect PARPi response in HGSOC. Our data suggest that bromodomain functions of HAT proteins such as PCAF, or accessory proteins such as BRPF3, may play a greater role in PARPi response than acetyltransferase functions.

Keywords: HGSOC, ovarian cancer, PARP inhibitor, resistance, H3K14ac, BRPF3

Background

High grade serous ovarian carcinoma (HGSOC) is the deadliest gynecological malignancy. It is the fifth most common cause of cancer death in women and has one of the highest death-to-incidence ratios of all cancers (1). Most patients initially respond to standard-of-care cytoreductive surgery and platinum/taxol chemotherapy. The addition of PARP inhibitors (PARPi) as first-line maintenance therapy, supported by numerous clinical trials in homologous recombination-deficient and -proficient cohorts, has extended progression-free survival intervals for many patients (2-4). Despite these advances, over 80% of cases recur and are expected to acquire resistance to all available therapies. Since nearly all HGSOC patients will be eligible to receive PARPi, it is essential to discover mechanisms of resistance and provide support for novel therapies to overcome resistance and improve outcomes.

Numerous studies and trials have focused on exploiting vulnerabilities to augment or restore PARPi sensitivity, including the use of topoisomerase inhibitors (5, 6), cyclin-dependent kinase knockdown or inhibition (7, 8), Wnt inhibitors (9), and histone methyltransferase (HMT) inhibitors (10), among others [reviewed in (11)]. In the current study we examine histone modifications and expression of histone modifying enzymes in the context of PARPi-resistant HGSOC. Histone modifications play critical roles in PARPi resistance, as they control access to genomic DNA for vital processes including transcription, replication, and repair (12, 13). When dysregulated, these same modifications have been shown to contribute to every aspect of cancer biology, from early oncogenesis to progression, metastasis, chemoresistance, and immune evasion (14-17). Acetylation of histone H3 lysine 14 (H3K14ac) neutralizes the positively charged lysine residue and reduces interactions between the histone octamer and encircling DNA, thus allowing greater access for transcriptional, replicative, and DNA repair machinery (18, 19). As such, H3K14ac is generally a modification associated with transcriptionally active chromatin.

While H3K14ac is only a single modification, its regulation is complex, as it may be catalyzed by numerous histone acetyltransferases (HATs) of different classes including (but not limited to) GCN5 and PCAF (encoded by *KAT2A* and *KAT2B*, respectively), CBP and P300 (encoded by *KAT3A* and *KAT3B*, respectively), as well as HBO1, also known as MYST2 (*KAT7*). H3K14ac is known to be an important factor in the process of single-stranded DNA break (SSB) and double-stranded DNA break (DSB) repair. For SSB repair, H3K14 acetylation stabilizes chromatin interactions and promotes error-free Nucleotide Excision Repair (NER) (20). The structurally similar HATs PCAF and GCN5 promote repair by acetylation of H3K14, and also by acetylation of non-histone targets including Replication Protein A1 (RPA1) (21). Acetylation of RPA1 by PCAF/GCN5 activates NER and promotes accumulation of DNA repair proteins at sites of damage. For DSB, histone acetylation by structurally similar HATs P300 and CBP promote chromatin remodeling and recruitment of effectors involved in both homologous recombination (HR) and non-homologous end joining (NHEJ) (22, 23). Additionally, P300/CBP promote transcription of HR factors BRCA1 and RAD51 recombinase (24). Finally, phosphorylated HBO1 has been shown to facilitate recruitment of the NER protein XPC to sites of cyclopyrimidine dimers (CPD) and is essential for NER at sites of ultraviolet (UV) irradiation damage (25).

Modifiers of histone acetylation, especially histone deacetylases (HDACs) and HDAC inhibitors, have been investigated as therapeutic targets in HGSOC [reviewed in (26)]. However, prior to this report, the roles of H3K14ac and these specific HAT enzymes in PARPi resistance had not been examined in HGSOC.

Results

H3K14ac enrichment and expression of histone acetyltransferases are altered in PARPi-resistant HGSOC cell lines and PDX models

Four *TP53*-mutated HGSOC cell lines (PEO1, OVSAHO, Kuramochi, and OVCA433) were subjected to stepwise dose escalation of olaparib to select for resistant cells. PEO1, OVSAHO, and Kuramochi are *BRCA2*-mutated, while OVCA433 are *BRCA1/2*-wildtype. Olaparib resistance was confirmed in each line using dose response colony formation assays. Olaparib response in PEO1 (IC_{50} = 6.4 nM) and PEO1-OR (IC_{50} = 1223 nM), and mechanisms of resistance have been reported (9, 10). Olaparib response curves and IC_{50} values for OVSAHO-OR, Kuramochi-OR, and OVCA433-OR are shown in **Supplemental Fig. S1**. Histones from each parental and olaparib-resistant line were isolated and histone H3 and H4 modifications were examined via mass spectrometry. We reported these data for PEO1/PEO1-OR (10), and we include these data for comparison with the three new sensitive/resistant isogenic pairs. Notably, H3K14ac was significantly altered in all four resistant lines compared to the parental lines **(Fig. 1A)**. Compared to the sensitive counterpart, H3K14ac was elevated in PEO1-OR, OVSAHO-OR, and OVCA433-OR, but decreased in Kuramochi-OR. Complete mass spectrometry data for PEO1/PEO1-OR are published (10), and data for all marks analyzed in the remaining lines are available in **Supplemental File 1**. We isolated histones from each cell line pair and confirmed these results by immunoblotting for H3K14ac and normalizing band intensity to total H3 **(Fig. 1B)**.

We next examined expression of histone acetyltransferases (HATs) in each sensitive/resistant cell line pair. We examined expression of five HATs with known H3K14 acetylation activity by RT-qPCR, including *KAT3B* (P300), *KAT3A* (CBP), *KAT2B* (PCAF), *KAT2A* (GCN5), and *KAT7* (HBO1) (27-32). We found significantly different expression of at least two HATs in each cell line **(Fig. 1C)**. For example, PEO1-OR showed upregulation of all HATs except *KAT3B* relative to the olaparib-sensitive PEO1 cells. None of the HATs were predictive of up- or down-regulation of H3K14ac in the resistant cell lines. For example, *KAT7* was upregulated in PEO1-OR, Kuramochi-OR, and OVCA433-OR, but H3K14ac was

significantly decreased in Kuramochi-OR, while being increased in the other olaparib-resistant lines.

We utilized GTFB-PDX1009, a BRCA-wildtype patient-derived xenograft (PDX) model of HGSOC to establish an additional olaparib-resistant model. Following intraperitoneal injection of primary HGSOC ascites samples into immunocompromised NOD SCID gamma (NSG) mice, tumor bearing mice were treated daily with olaparib or vehicle control for 21 days and the mice were monitored for two months [schematic published in (10)]. After recurrence and necropsy, tumor cells isolated from olaparib-treated mice were subsequently shown to be highly olaparib-resistant (9). We published that histone methyltransferases EHMT1 and EHMT2 were upregulated in the olaparib-resistant PDX (10). By RT-qPCR, we found that mRNA expression of *KAT3A* and *KAT2A* were increased in all four olaparib-treated ascites, while *KAT2B* and *KAT3B* were upregulated in one and two mice, respectively **(Fig. 1D)**. We further performed RNA-Seq to compare the transcriptomes of control mice (#834 and #836) with two olaparib-treated mice (#827 and #878). RNA-Seq data confirmed significant upregulation of *KAT2A* (GCN5) and *KAT3A* (CBP) in the olaparib-treated mice **(Supplemental Table S1)**. In summary, H3K14 acetylation and HAT expression are altered in PARPi-resistant models of HGSOC, including *BRCA*-deficient and -proficient cell lines, as well as a BRCA-proficient PDX.

Genetic knockdown of HATs in olaparib-resistant HGSOC cells moderately alters olaparib response

As stated above, H3K14ac is associated with multiple DNA repair mechanisms. Augmented DNA repair is an important component of PARPi resistance (11), and we have previously shown that knockdown or inhibition of epigenetic enzymes such as histone methyltransferases can significantly improve olaparib response (10). We therefore chose to knock down each HAT highlighted in **Fig. 1C** and examine olaparib response. Since PEO1-OR showed upregulation of 4 of the 5 HATs, we used lentiviral transduction to stably express

shRNAs targeting each HAT, or a non-targeting scrambled shRNA as control (shCTRL), in these cells. We determined the degree of knockdown for each shRNA relative to shCTRL by RT-qPCR **(Fig. 2A-E)**. We then performed dose response colony formation assays. Cells were treated with vehicle control or doses of olaparib ranging from 4.8 nM to 30 μM and the olaparib IC_{50} was calculated for each shRNA **(Fig. 2F-J and Table 1)**. Both shRNA against *KAT3B* (P300), one shRNA against *KAT3A* (CBP), and both shRNA against *KAT2A* (GCN5) significantly reduced the olaparib IC50 relative to shCTRL, although in all cases the level of sensitization was modest. Despite differing levels of knockdown, both shRNA against *KAT2B* (PCAF) increased olaparib IC_{50} in PEO1-OR cells, with sh*KAT2B*#1 showing a significant increase of 174% relative to shCTRL. This was a surprising result, as PCAF levels are increased in PEO1-OR cells relative to sensitive PEO1. Neither shRNA targeting *KAT7* (HBO1) showed a significant effect. Olaparib IC_{50} for all shRNA are shown in **Table 1**. Depending on the shRNA and target, shifts of olaparib response were generally modest, with a surprising increase in olaparib IC_{50} observed with knockdown of PCAF.

Depletion of H3K14ac does not sensitize olaparib-resistant HGSOC cells, but bromodomains may play roles in olaparib response

We next determined if depletion of H3K14ac was sufficient to sensitize PEO1-OR cells to olaparib. We determined that 10 μM HBO1 inhibitor WM-3835, characterized by MacPherson *et al.* (33), severely depleted H3K14ac. By immunoblot densitometry, only 27% of H3K14ac remained in PEO1-OR cells after a 6-hour incubation **(Fig. 3A)**. We then performed colony formation assays using olaparib alone or in combination with 10 μM WM-3835. Despite the efficacy of H3K14ac depletion, no change in olaparib IC_{50} was found between the two treatments **(Fig. 3B and Table 2)**. Rather than continuing with direct inhibition of acetyltransferase activity, we elected to test if inhibition of the bromodomains (BRD) of HAT enzymes had an effect on olaparib response. We performed colony formation assays in PEO1-

OR using olaparib alone or in combination with 2 μM GCN5/PCAF BRD inhibitors L-Moses or GSK4027, or 2 μM P300/CBP BRD inhibitor SGC-CBP30. L-Moses and SGC-CBP30 had no effect on olaparib IC_{50}, while GSK4027 notably increased olaparib resistance in PEO1-OR cells **(Fig. 3C and Table 2)**. This agrees with our data showing that knockdown of PCAF also increases olaparib resistance in these cells.

While the PCAF bromodomain may play a role in olaparib response, it must be noted that the GCN5/PCAF BRDs also read H3K36 acetylation and the P300/CBP BRDs read H3K56 acetylation (34). We therefore chose to specifically inhibit the bromodomains of proteins that have direct reading function of H3K14ac. These include Bromodomain Adjacent to Zinc Finger Domain 2B (BAZ2B) and proteins in the Bromodomain and PHD-Finger Containing (BRPF)-family (34). We performed colony formation assays in PEO1-OR cells using olaparib alone or in combination with 2 μM BAZ2B inhibitors BAZ2-ICR or GSK2801, or 2 μM pan-BRPF inhibitors NI-57 or OF-1 **(Fig. 3D)**. Much like inhibition of PCAF, inhibition of BAZ2B with BAZ2-ICR significantly increased olaparib resistance. However, inhibition of BRPF family proteins by OF-1 significantly decreased the olaparib IC_{50}. Olaparib IC_{50} and p-values for all inhibitor treatments are shown in **Table 2**.

BRPF3 is elevated in HGSOC and associated with poor outcomes, and may play a role in olaparib response

BRPF3 is notable among the BRPF family proteins for a known association with HBO1, in which it directs a multiprotein complex toward acetylation of H3K14, rather than lysines of histone H4 (35). We examined a publicly available microarray dataset comparing mRNA expression in normal fallopian tube epithelium (FTE) versus HGSOC. *KAT7* (HBO1) trended toward elevated mRNA levels in HGSOC **(Fig. 4A)** but did not quite reach significance. *BRPF3* was significantly elevated in HGSOC compared to normal FTE **(Fig. 4B)**. We also analyzed a TCGA microarray dataset of ovarian tumors and analyzed overall survival. Using KMplot (36)

we split a cohort of patients into low or high expression of *KAT7* **(Fig. 4C)** or *BRPF3* **(Fig. 4D)**. We observed that high *KAT7* expressing patients trended toward longer overall survival, but again did not reach significance. High *BRPF3* expressing patients, however, showed significantly shorter overall survival than low *BRPF3* expressing patients. We used the Cancer Science Institute of Singapore Ovarian Database (CSIOVDB) to perform a further meta-analysis of HGSOC microarray data (37-39). *BRPF3* was significantly upregulated in higher stage and grade of HGSOC **(Supplemental Fig. S2)**. A meta-analysis using canSAR Black (40) showed BRPF3 has the strongest association with ovarian cancer in combined molecular score, which includes mutation score, gene expression, and copy number variation score **(Supplemental Fig. S3)**.

We examined *BRPF3* mRNA expression in our four olaparib-sensitive/-resistant cell line pairs. It was increased in PEO1-OR vs sensitive PEO1 but decreased in OVCA433-OR vs sensitive OVCA433 **(Fig. 4E)**. *BRPF3* was also modestly upregulated in olaparib-treated ascites of GTFB-PDX1009 **(Supplemental Table S1)**. We again used lentiviral transduction to stably express shCTRL or shRNAs targeting *BRPF3* in PEO1-OR. We determined the degree of knockdown for each shRNA relative to shCTRL by RT-qPCR **(Fig. 4F)** and Western blot **(Fig. 4G)**. While mRNA expression appeared similar between the two *BRPF3* shRNA lines, the amount of protein in sh*BRPF3#2* was notably lower. We next compared olaparib response in *BRPF3* knockdown cells compared to control. Olaparib IC_{50} for shCTRL in this experiment was 1036 nM. sh*BRPF3*#1 (IC_{50} = 938 nM, p = 0.517) did not significantly alter olaparib IC_{50} in PEO1-OR. However, in agreement with better knockdown, sh*BRPF3#2* (IC50 = 479 nM, p = 0.0002) did significantly reduce the olaparib IC_{50} **(Fig. 4H)**.

Discussion

Regardless of BRCA status, numerous clinical trials show that PARPi have significant benefit to both newly diagnosed and recurrent HGSOC cases (2, 3, 41). Going forward, nearly

all HGSOC patients will be eligible to receive PARPi, and it is essential to identify and specifically target novel vulnerabilities to improve response rates and increase the number of patients who can benefit from PARPi treatment. PARPi cause ssDNA breaks and can cause replication fork collapse due to altered fork speed and stability (42, 43). Epigenetic modifications and enzymes are likely to be important mechanisms of PARPi resistance, as they control access to DNA for transcription, replication, and repair. In this report, we employed an unbiased proteomic approach to profile the epigenetic landscape of four PARPi-resistant HGSOC cells, including BRCA-deficient and -proficient lines. We observed altered enrichment of H3K14ac in all four PARPi-resistant lines compared to isogenic PARPi-sensitive cells **(Fig. 1A-B)**. Gene expression of HATs was also altered in PARPi-resistant lines, as well as in a PDX model of PARPi-treated HGSOC **(Fig. 1C-D)**. Using both genetic and pharmacologic approaches, we examined if depletion or inhibition of specific HATs or accessory bromodomain (i.e., H3K14ac reader) proteins altered the response to the PARPi olaparib. Notably, severe pharmacologic depletion of H3K14ac did not affect PARPi response. However, knockdown or inhibition of PCAF increased PARPi resistance. Knockdown and inhibition of BRPF3, a bromodomain protein associated with HBO1, modestly sensitized HGSOC cells to olaparib.

Placing this work in the context of prior studies, we reported an epigenetic mechanism of PARPi resistance in HGSOC. Specifically, we showed that H3K9me2 was enriched in PARPi-resistant HGSOC cell line and PDX models, concomitant with upregulation of euchromatic histone-lysine N-methyltransferase-1 and -2 (EHMT1 and EHMT2), the enzymes responsible for writing the H3K9me2 mark (10). Genetic knockdown or pharmacologic inhibition of EHMT1/2 sensitized PARPi-resistant HGSOC cells and ablated both HR and NHEJ DNA repair. H3K9 methylation is known to be linked to H3K14ac by the triple Tudor domain of SETDB1, which may play a role in silencing of active genomic regions (44). We observed significant upregulation of both H3K9me2 and H3K14ac in PEO1-OR cells relative to parental, olaparib-sensitive PEO1. Profiling studies such as chromatin immunoprecipitation (ChIP) will be required

to determine if regions of these two marks overlap. H3K9me2 was not as strongly upregulated in the three other olaparib-resistant lines, suggesting that a strong linkage of H3K9 methylation with H3K14ac may exist only in a subset of HGSOC. Further studies will be necessary to test the efficacy of combined inhibition of EHMT1/2 with HAT or BRD inhibitors.

Knockdown of specific HATs had only modest effects at sensitizing PEO1-OR to olaparib **(Fig. 2)**. Despite PCAF being upregulated in PEO1-OR cells relative to olaparib-sensitive PEO1, knockdown of PCAF further increased olaparib resistance **(Fig. 2H)**. A prior study showed that acetylation of RPA1 by PCAF/GCN5 promoted NER (21), so we would expect knockdown of PCAF and/or GCN5 to lessen DNA repair and promote PARPi sensitivity. However, another study showed that PCAF and CBP/P300 acetylate p53 in response to DNA damage (45). We may surmise that the presence of *TP53* mutations in nearly all HGSOC cases could alter this response, but further study is required.

The severe depletion of H3K14ac by HBO1 inhibitor WM-3835 indicates that the majority of H3K14 acetylation in PEO1-OR cells is mediated by HBO1 **(Fig. 3A)**. A prior study demonstrated that HBO1 was enriched on the transcriptional start sites of actively transcribed genes, and that HBO1 contributed to bulk histone acetylation at these sites (46). In that study, HBO1 enrichment correlated with the level of promoter H3K14 acetylation. Given that the addition of 10 μM WM-3835 did not affect the olaparib IC_{50} in PEO1-OR **(Fig. 3B)**, we conclude that the acetyltransferase activity of HBO1, and bulk H3K14 acetylation, do not have a major effect on PARPi response. Our data also suggest that the genes regulated by HBO1-mediated H3K14ac are not involved in PARPi response. However, the prior study also showed that HBO1 enrichment, despite being correlated with H3K14ac, did not correlate with transcription levels of specific genes. Thus, even though WM-3835 severely depletes H3K14ac, transcriptional data would be needed to determine if WM-3835 had significant effects on transcription. Further, despite other HATs having a lesser role in bulk genomic H3K14ac, it is possible that other HATs acetylate histones at other genomic locations and genes, some of which may alter PARPi

response. We must also consider that acetylation of non-histone targets by other HATs may have effects on PARPi response. ChIP studies of specific loci, and specific targeting with other HAT inhibitors will be required to tease out precise effects.

Unlike HBO1 acetyltransferase inhibition, the use of BRD inhibitors did affect olaparib response. PCAF bromodomain inhibitor GSK2027 increased olaparib resistance in PEO1-OR **(Fig. 3C)**, which agrees with increased olaparib IC_{50} in PCAF knockdown cells **(Fig. 2B)** and indicates that the bromodomain of PCAF, rather than the HAT domain, may play a significant role. Also, despite being readers of the same H3K14ac mark, inhibition of BAZ2B or BRPF-family proteins had opposite effects on olaparib response. Inhibition of BAZ2B with both BAZ2-ICR increased resistance, while inhibition of the BRPF family with OF-1 decreased resistance **(Fig. 3D)**, demonstrating the highly complex regulatory nature of histone modifications. Overall, we found that the blunt method of HBO1 inhibition was ineffective at reversing PARPi resistance. Changes in IC_{50} due to BRD inhibition suggest that histone readers and other accessory factors in acetyltransferase protein complexes may play a greater role in PARPi response than the HATs themselves. The exact subunit composition of such complexes in HGSOC, and how these may be altered in acquired PARPi resistance, remain unknown.

This concept is further emphasized by the increased expression of *BRPF3* in HGSOC compared to normal FTE **(Fig. 4B)** and the association of elevated *BRPF3* expression with higher ovarian cancer stage and grade **(Supplemental Fig. S2)**, and with worse overall survival **(Fig. 4D)**. While OF-1 is a pan-BRPF inhibitor, specific knockdown of BRPF3 effectively reduced olaparib IC_{50} in PEO1-OR, indicating its importance in PARPi response. The protein complex containing BRPF3 and HBO1 has been shown to regulate H3K14 acetylation. BRPF3 was found to be crucial for H3K14 acetylation, as well as loading of CDC45 at DNA origins of replication and activation of those origins (47). Since PARPi-induced DSBs are generated during DNA replication at collapsed replication forks, this role of BRPF3 in DNA replication

suggests a possible mechanism for loss or inhibition of BRPF3 to sensitize olaparib-resistant cells.

Conclusions

Our reported findings highlight the altered epigenetic landscape of PARPi-resistant HGSOC, including histone modifications and changes in expression of associated epigenetic-modifying enzymes. While non-histone targets for acetylation have yet to be examined, our data suggest that the reader function of specific bromodomains may play a greater role than acetyltransferase domains. In conclusion, specific BRD proteins such as BRPF3, in association with HATs, may play a role in PARPi response even if total H3K14ac levels are not predictive or associated with resistance. Further examination of HAT complex composition in HGSOC, and the activities of each subunit, may reveal novel vulnerabilities.

Methods

Cell culture, shRNA, and lentivirus

Cell lines were obtained from the Gynecologic Tumor and Fluid Bank (GTFB) at the University of Colorado and were authenticated at the University of Arizona Genomics Core using short tandem repeat DNA profiling. Regular mycoplasma testing was performed using MycoLookOut PCR (Sigma). HGSOC lines were cultured in RPMI 1640 supplemented with 10% fetal bovine serum (FBS) and 1% penicillin/streptomycin. 293FT lentiviral packaging cells were cultured in DMEM supplemented with 10% FBS and 1% penicillin/streptomycin. All cells were grown at 37 °C supplied with 5% CO_2. shRNA in pLKO.1 lentiviral vector plasmid were purchased from the University of Colorado Functional Genomics Facility. Sequences and The RNAi Consortium numbers are listed in **Supplemental Table S2**. A scrambled non-targeting shRNA was used as control (Sigma-Aldrich #SHC016). Lentivirus was packaged as previously described (48) in 293FT using 3rd generation packaging plasmids (Virapower, Invitrogen) with polyethyleneimene

(PEI) transfection in a 1:3 DNA:PEI ratio. Culture supernatant was harvested at 48-72 h post-transfection and processed through 0.45 μM filters. Viruses encoded a puromycin resistance gene. Transduced HGSOC cells were selected in 1 μg/mL puromycin.

Histone modification profiling

Profiling of histone modifications in olaparib-sensitive and –resistant cells was performed by the Northwestern University Proteomics Core. Briefly, we provided frozen pellets of 5 x 10^6 PEO1 and PEO1-OR cells. Histone extracts were trypsin digested and histone residues were assayed as previously reported (49, 50) by liquid chromatography coupled to mass spectrometry using a TSQ Quantiva Ultra Triple Quadrupole Mass Spectrometer.

PDX mouse model of PARPi-resistant HGSOC

All animal experiments were performed in accordance with the Guide for the Care and Use of Laboratory Animals and were approved by the University of Colorado IACUC. Primary ovarian cancer sample GTFB1009 (BRCA1/2-wildtype) was provided by the University of Colorado Gynecologic Tumor and Fluid Bank. 6 to 8-week-old NOD SCID gamma (NSG) mice (Jackson Labs) were given intraperitoneal injections of 5 million GTFB1009 ascites cells each. Following a 7-day incubation period, mice were given once daily intraperitoneal injections of 50 mg/kg olaparib or vehicle control (10% 2-hydroxypropyl-β-cyclodextrin, Sigma-Aldrich #C0926) for 21 days. After treatment, tumors were allowed to recur for two months. Mice were then euthanized, and ascites were collected for analysis. This model is further characterized in (9).

RNA-Seq of GTFB-PDX1009

RNA was isolated from olaparib-treated (n = 2) and -untreated (n = 2) GTFB-PDX1009 ascites using the RNeasy Plus Mini kit (Qiagen). RNA quality was confirmed using an Agilent TapeStation and all RNA used for library preparation had a RIN>9. Libraries were generated

and sequencing was performed by Novogene. HISAT (51) was used for alignment against GRCh37 version of the human genome. Samples were normalized using TPM (Transcripts per Kilobase Million) measurement and gene expression using the GRCh37 gene annotation was calculated using home-made scripts. Analysis was performed by the Division of Translational Bioinformatics and Cancer Systems Biology at the University of Colorado School of Medicine. Data are available at accession GSE131231.

Compounds

P300/CBP inhibitor SGC-CBP30 (SelleckChem #S7256), PCAF inhibitors GSK4027 (Cayman #23421) and L-Moses (Tocris #6251), and BAZ2B inhibitors GSK2801 (SelleckChem #S7231) and BAZ2-ICR (Tocris #5266) were purchased from the indicated suppliers. HBO1 inhibitor WM-3835 was kindly provided by Jonathan Baell of the Monash Institute of Pharmaceutical Sciences (Victoria, Australia) and Professor Mark Dawson of the Peter MacCallum Cancer Centre, University of Melbourne (Melbourne, Australia).

Colony formation assay

2500 cells were seeded per well in 24-well plates and treated with increasing doses of olaparib alone or in combination with the indicated compounds. Media and drugs were changed every three days until control wells were confluent. Colonies were washed twice with PBS, then incubated in fixative (10% methanol and 10% acetic acid in PBS). Fixed colonies were stained with 0.4% crystal violet in 20% ethanol/PBS. After imaging, crystal violet was dissolved in fixative and absorbance was measured at 570 nm using a Molecular Devices SpectraMax M2e plate reader.

Reverse-transcriptase quantitative PCR (RT-qPCR)

RNA was isolated from cells using the RNeasy Plus Mini Kit (Qiagen). mRNA expression was determined using SYBR green Luna One Step RT-qPCR Kit (New England BioLabs) on a C1000 Touch (Bio-Rad) or QuantStudio 6 (Applied Biosystems) thermocycler. Expression was quantified by the ΔΔCt method using target-specific primers and glyceraldehyde 3-phosphate dehydrogenase (*GAPDH*) control primers. mRNA-specific primers were designed to span exon-exon junctions to avoid detection of genomic DNA. Primer sequences are shown in **Supplemental Table S3**.

Immunoblotting

For histone blots, extracts were made using the Histone Extraction Kit (Abcam #ab113476). For total protein, cells were lysed and briefly sonicated in RIPA buffer (150mM NaCl, 1% TritonX-100, 0.5% sodium deoxycholate, 0.1% SDS, 50mM Tris pH 8.0) supplemented with cOmplete EDTA-free protease inhibitors (Roche #11873580001) and phosphatase inhibitors NaF and Na_3VO_4. Protein was separated by SDS-PAGE and transferred to PVDF membrane using the TransBlot Turbo (BioRad). Membranes were blocked in LI-COR Odyssey buffer (#927-50000) for 1 hour at room temperature. Primary antibody incubation was performed overnight in blocking buffer at 4 °C. Membranes were washed 3 times for 5 minutes each in TBST (50 mM Tris pH 7.5, 150 mM NaCl, 0.1% Tween-20), then secondary antibodies were applied in blocking buffer for one hour at room temperature. Membranes were washed again 3 times for 5 minutes each in TBST. Bands were visualized using the LI-COR Odyssey Imaging System. Primary antibodies were: H3K14ac (Cell Signaling #7627, Rabbit, 1:1000), total H3 (Cell Signaling #14269, Mouse, 1:1000), BRPF3 (Abcam #ab69410, Mouse, 1:1000), and β-actin (Abcam #ab6276, Mouse, 1:10,000). Secondary antibodies were LI-COR fluorophore-labeled secondary goat anti-rabbit (IRDye 680RD or IRDye 800CW, #925-68071 or #926-32211) or goat anti-mouse (IRDye 680RD or IRDye 800CW, #926-68070 or #925-32210) at 1:20,000 dilution.

Densitometry

For immunoblot images captured using the LI-COR Odyssey, band fluorescence intensity was analyzed using LI-COR ImageStudio 4. Immunoblots of histone extracts were normalized to band intensity of total H3. Immunoblots of total protein lysates were normalized to intensity of β-actin.

Ovarian cancer dataset analysis

Microarray data from publicly available ovarian cancer database GSE10971 (52, 53) was analyzed to compare gene expression between normal fallopian tube epithelium and high grade serous ovarian carcinoma. KMplot (36) was used to interrogate TCGA ovarian cancer gene expression data and compare overall survival in high and low expressing patients. CSIOVDB (37-39) and canSAR Black (40) were used to further interrogate associations between *BRPF3* and ovarian cancer microarray datasets.

Software and statistical analysis

Statistical analysis and calculation of P value was performed using GraphPad Prism. Quantitative data are expressed as mean ± SD unless otherwise stated. Two-tailed t-test was used for single comparisons. Analysis of variance (ANOVA) with Fisher's Least Significant Difference (LSD) was used in multiple comparisons. Olaparib IC_{50} were calculated and compared using the Nonlinear regression (curve fit) analysis, log(inhibitor) vs. response (three parameters) model, with extra sum-of-squares F-test. For all statistical analyses, the level of significance was set at 0.05.

Declarations

Ethics approval and consent to participate: N/A

Consent for publication: N/A

Availability of data and materials: Data generated and/or analyzed during this study are available from the corresponding author(s) on reasonable request. RNA-Seq dataset(s) are deposited as described in materials and methods and are publicly available.

Competing interests: The authors declare that they have no competing interests.

Funding: We acknowledge philanthropic contributions from the Kay L. Dunton Endowed Memorial Professorship in Ovarian Cancer Research, the McClintock-Addlesperger Family, Karen M. Jennison, Don and Arlene Mohler Johnson Family, Michael Intagliata, Duane and Denise Suess, Mary Normandin, and Donald Engelstad. This work was supported by The Department of Defense Ovarian Cancer Research Program (BGB, OC170228, OC200302, OC200225; ZLW, OC210257), The American Cancer Society (BGB, RSG-19-129-01-DDC), the NIH/National Cancer Institute (BGB, R37CA261987; ZLW, R03CA249571), the Cancer League of Colorado (BGB, 183478-BB; ZLW, 193527-ZW), and the Colorado Clinical & Translational Sciences Institute (ZLW, CCTSI CO-Pilot CO-J-20-006). Use of the University of Colorado Functional Genomics Facility was supported by NCI grant P30CA046934, and by NIH/NCATS Colorado CTSA Grant Number UL1TR002535. Histone profiling was performed by the Northwestern University Proteomics Core, supported by NCI CCSG P30CA060553 and P41GM108569.

Author's contributions: ZLW designed the study, performed experiments, analyzed and interpreted data, and prepared and revised the manuscript. TMY and AM generated olaparib-resistant cell lines, characterized the PDX model, and edited the manuscript. HK analyzed RNA-Seq data. BGB aided in study design, data analysis and interpretation, and manuscript preparation and revision.

Acknowledgements

We acknowledge Professor Jonathan Baell of the Monash Institute of Pharmaceutical Sciences (Victoria, Australia) and Professor Mark Dawson of the Peter MacCallum Cancer Centre, University of Melbourne (Melbourne, Australia) and their labs for their generous gift of HBO1 inhibitor WM-3835.

TABLE 1

shRNA	Olaparib IC_{50} (nM)	% shCTRL	P-value
shCTRL	2620	-	-
sh*KAT3B* #1	1699	65%	0.016
sh*KAT3B* #2	1716	65%	0.021
sh*KAT3A* #1	1672	64%	0.014
sh*KAT3A* #2	1955	75%	0.099
sh*KAT2B* #1	4549	174%	0.002
sh*KAT2B* #2	3409	130%	0.105
sh*KAT2A* #1	1104	42%	< 0.0001
sh*KAT2A* #2	1704	65%	0.009
shRNA	**Olaparib IC_{50} (nM)**		
shCTRL	1593	-	-
sh*KAT7* #1	1431	90%	0.444
sh*KAT7* #2	1348	85%	0.352

Table 1. Olaparib IC_{50} values of control and HAT knockdown PEO1-OR HGSOC cells. For each indicated shRNA, the olaparib IC_{50} values are shown. Also shown are IC_{50} percentage relative to shCTRL (% shCTRL) and p-value.

TABLE 2

Compound(s)	Olaparib IC_{50} (nM)	% Olap.	P-value
Olaparib Only	2479	-	-
Olap. + 10 μM WM-3835	2668	108%	0.711
Compound(s)	**Olaparib IC_{50} (nM)**	**% shCTRL**	**P-value**
Olaparib Only	2280	-	-
Olap. + 2 μM L-Moses	2433	107%	0.739
Olap. + 2 μM GSK4027	3540	155%	0.019
Olap. + 2 μM SGC-CBP30	2488	109%	0.719
Compound(s)	**Olaparib IC_{50} (nM)**	**% shCTRL**	**P-value**
Olaparib Only	2436	-	-
Olap. + 2 μM BAZ2-ICR	6547	269%	< 0.0001
Olap. + 2 μM GSK2801	3401	140%	0.108
Olap. + 2 μM NI-57	3201	131%	0.151
Olap. + 2 μM OF-1	1379	57%	0.016

Table 2. Olaparib IC_{50} values of PEO1-OR HGSOC cells treated with olaparib alone or in combination with 2 μM bromodomain inhibitors. For each treatment, the olaparib IC_{50} values are shown. Also shown are IC_{50} percentage relative to olaparib alone (% Olap.) and p-value.

FIG. 1

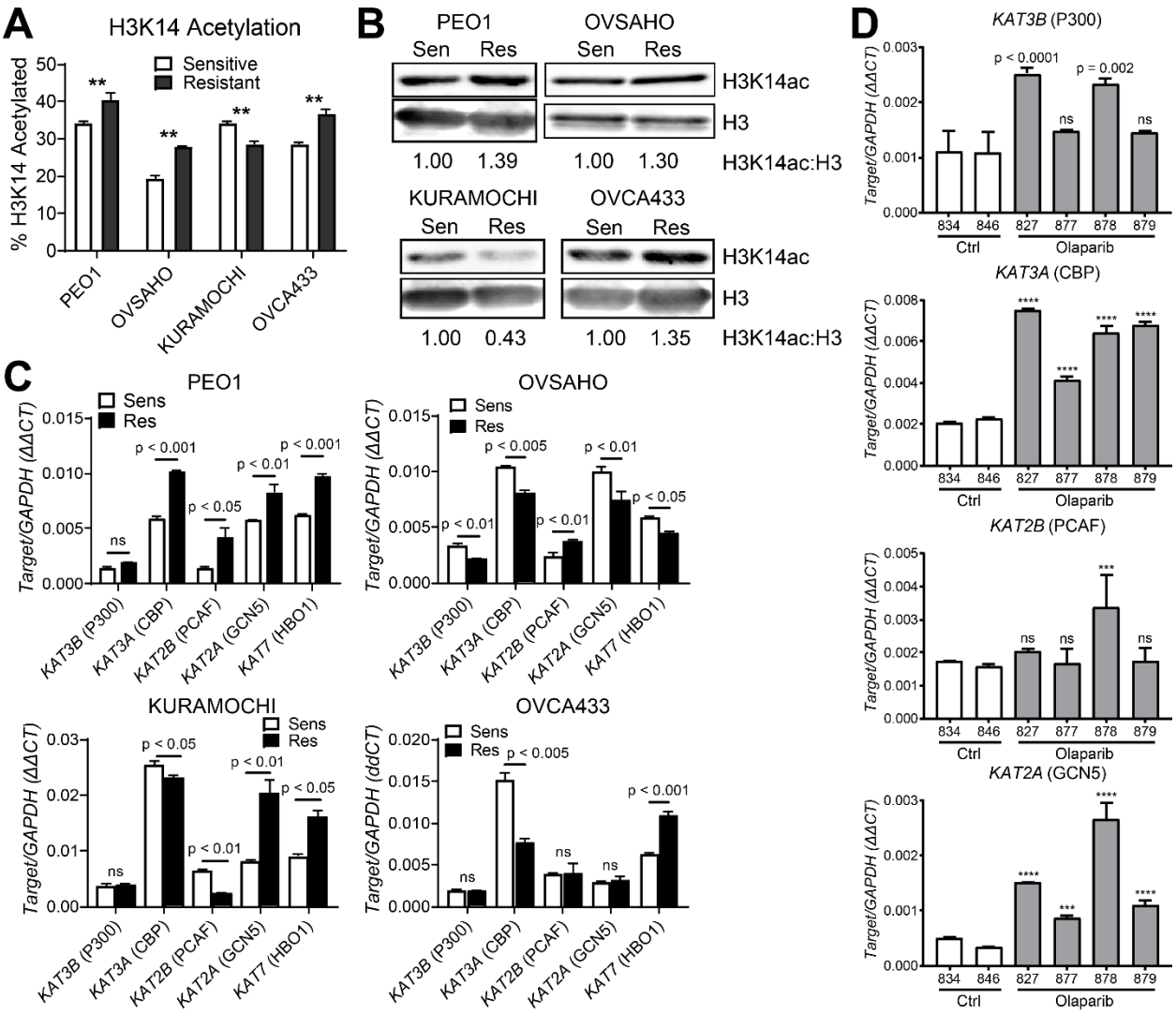

FIG 1. H3K14ac enrichment and histone acetyltransferase expression is altered in olaparib-resistant HGSOC cells and a PDX model. (A) Histone extracts from the indicated olaparib-sensitive and olaparib-resistant HGSOC cell lines were assayed by mass spectrometry for histone modifications. The percentage of acetylated H3K14 is shown for each sensitive/resistant pair. **(B)** Histone extracts from the indicated olaparib sensitive/resistant pairs were assayed by Western blotting for H3K14ac and total H3. The H3K14ac:H3 ratio was determined by band densitometry and normalized to the olaparib-sensitive line of each pair. **(C)** mRNA from the indicated olaparib-sensitive/-resistant pairs was assayed for HAT expression by

RT-qPCR. Target gene expression was determined relative to *GAPDH* control by ΔΔCt method. Each data point represents the average of three PCR reactions. P-values by T-test. **(D)** Human HGSOC PDX cells were injected into NSG mice. After seven days, mice received a 21-day treatment course of intraperitoneal vehicle control or 50 mg/kg olaparib. Following treatment, tumor cells were allowed to recur over an addition 21 days. Upon necropsy, ascites cells were collected. mRNA from ascites cells was analyzed by RT-qPCR for the indicated HATs. Target gene expression was determined relative to *GAPDH* control by ΔΔCt method. Each data point represents the average of three PCR reactions. Numbers below bars are mouse ear tag IDs. P-values were determined by T-test comparing each olaparib-treated mouse (gray bars; #827, #877, #878, or #879) to the average of both control mice (white bars; #834 and #846). *** $p < 0.001$; **** $p < 0.0001$.

FIG. 2

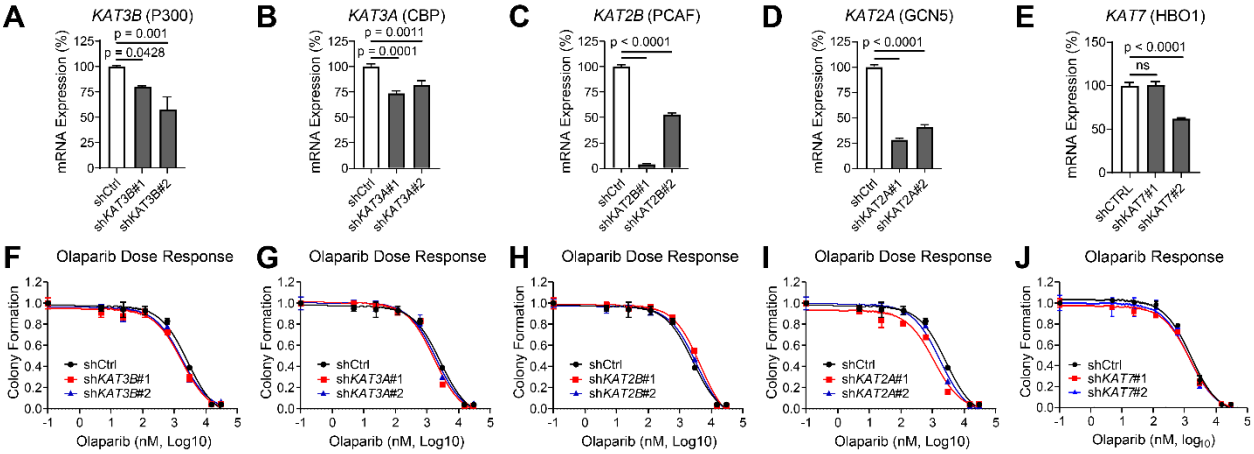

FIG 2. Knockdown of HATs shows only moderate alteration of olaparib response in PEO1-OR (olaparib-resistant) HGSOC cells. (A-E) PEO1-OR cells were transduced with the indicated targeted shRNAs or a non-targeting scrambled shRNA (shCTRL) and then selected in puromycin. Knockdown of each HAT was determined by RT-qPCR. mRNA expression was determined relative to *GAPDH* by ΔΔCt method, then normalized to shCTRL for each knockdown. P-value by T-test. **(F-J)** Each shRNA line was seeded at 2500 cells per well in a 24-well plate and treated with vehicle control or increasing doses of olaparib for eight days, after which colonies were fixed and stained with crystal violet. Stain was dissolved and the absorbance from each well was read by spectrophotometer, then normalized to vehicle control.

FIG. 3

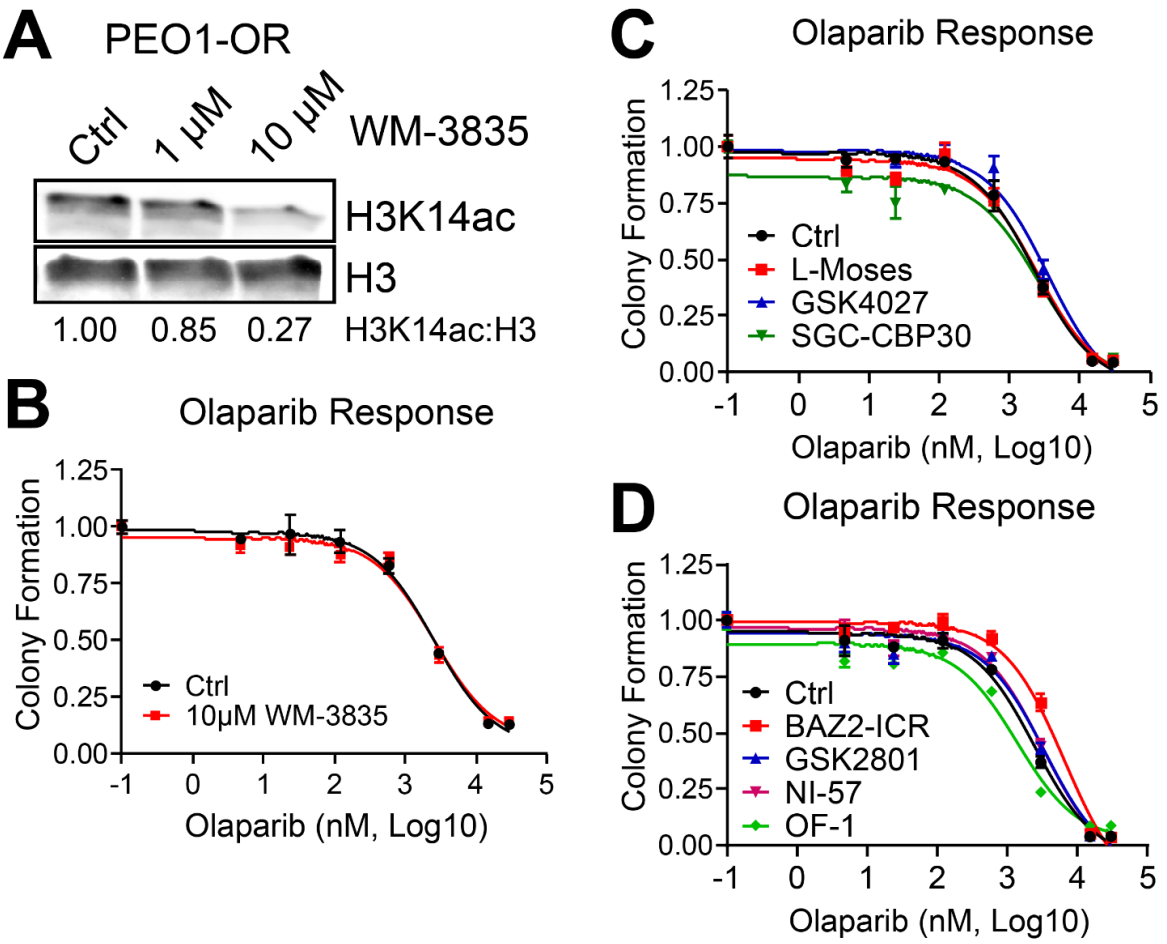

FIG 3. Depletion of H3K14ac does not shift olaparib IC_{50}, but BRD inhibitors moderately affect olaparib response in PEO1-OR HGSOC cells. (A) PEO1-OR cells were treated with the indicated doses of HBO1 acetyltransferase inhibitor WM-3835 for 6 hours. Histone extracts were analyzed by Western blot for H3K14ac and total H3. **(B)** PEO1-OR in a 24-well plate were treated with increasing doses of olaparib with or without 10 μM WM-3835. Colony formation and olaparib IC_{50} were determined as described for **Fig. 2F-J**. **(C-D)** PEO1-OR cells in a 24-well plate were treated with increasing doses of olaparib with or without 2 μM of the indicated bromodomain inhibitors. Colony formation and olaparib IC_{50} were determined as described for **Fig. 2F-J**.

FIG. 4

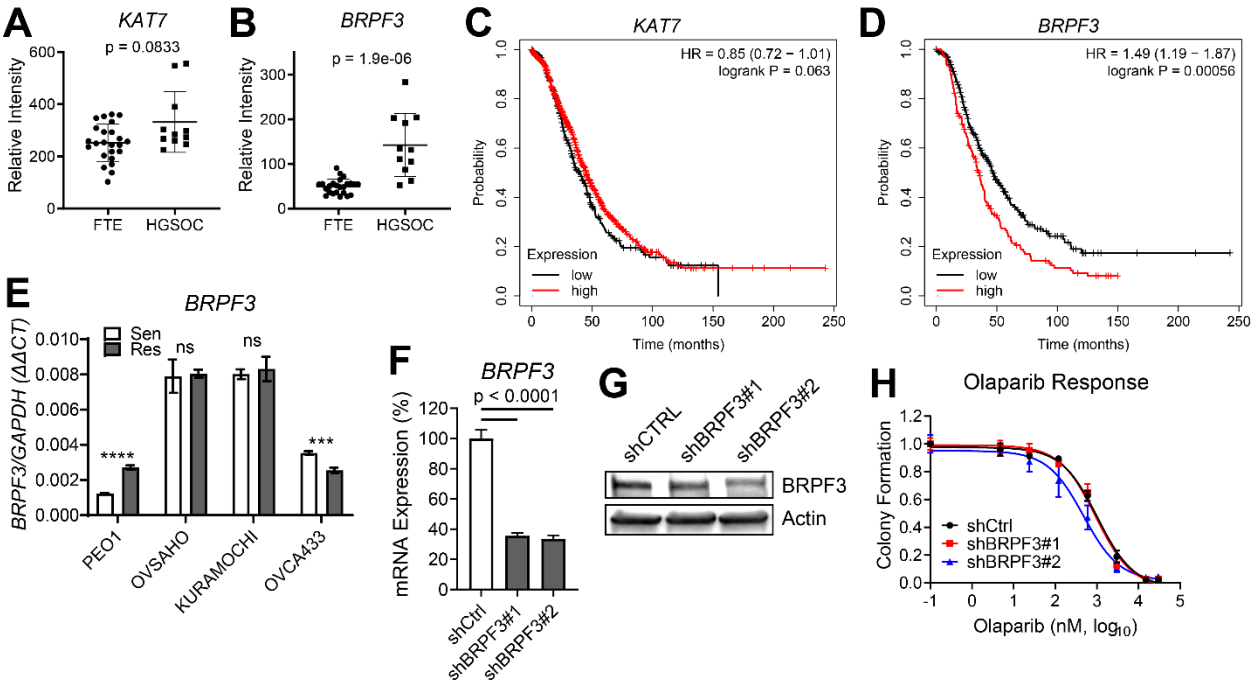

FIG 4. *BRPF3* mRNA expression is elevated in HGSOC relative to normal fallopian tube, and elevated expression is associated with worse overall survival. *BRPF3* knockdown moderately sensitizes PEO1-OR cells to olaparib. (A-B) mRNA expression of *KAT7* and *BRPF3* in microarray dataset GSE10971 was compared between HGSOC and normal FTE. P-value by T-test. **(C-D)** TCGA microarray data for *KAT7* and *BRPF3* were analyzed using KMplot and Kaplan-Meier curves were generated for overall survival (N = 655) of High and Low expressing patients for each gene. **(E)** mRNA from the indicated olaparib sensitive/resistant pairs was assayed for *BRPF3* expression by RT-qPCR. Target gene expression was determined relative to *GAPDH* control by ΔΔCt method. Each data point represents the average of three PCR reactions. P-values by T-test. *** $p < 0.001$; **** $p < 0.0001$. **(F-G)** PEO1-OR cells were transduced with shRNAs targeting *BRPF3* or a non-targeting scrambled shRNA (shCTRL) and then selected in puromycin. Knockdown of *BRPF3* was determined by RT-qPCR **(F)** and Western blotting **(G)**. mRNA expression in **(F)** was determined relative to *GAPDH* by ΔΔCt

method, then normalized to shCTRL for each knockdown. P-value by T-test. **(H)** Cells from **F-G** were treated with increasing doses of olaparib, and colony formation was assayed as in **Fig. 2C**.

References

1. Siegel RL, Miller KD, Jemal A. Cancer statistics, 2018. CA: a cancer journal for clinicians. 2018;68(1):7-30.
2. Moore K, Colombo N, Scambia G, Kim BG, Oaknin A, Friedlander M, et al. Maintenance Olaparib in Patients with Newly Diagnosed Advanced Ovarian Cancer. The New England journal of medicine. 2018.
3. Domchek SM, Aghajanian C, Shapira-Frommer R, Schmutzler RK, Audeh MW, Friedlander M, et al. Efficacy and safety of olaparib monotherapy in germline BRCA1/2 mutation carriers with advanced ovarian cancer and three or more lines of prior therapy. Gynecologic oncology. 2016;140(2):199-203.
4. Matulonis UA, Penson RT, Domchek SM, Kaufman B, Shapira-Frommer R, Audeh MW, et al. Olaparib monotherapy in patients with advanced relapsed ovarian cancer and a germline BRCA1/2 mutation: a multistudy analysis of response rates and safety. Ann Oncol. 2016;27(6):1013-9.
5. Patel AG, Flatten KS, Schneider PA, Dai NT, McDonald JS, Poirier GG, et al. Enhanced killing of cancer cells by poly(ADP-ribose) polymerase inhibitors and topoisomerase I inhibitors reflects poisoning of both enzymes. The Journal of biological chemistry. 2012;287(6):4198-210.
6. Znojek P, Willmore E, Curtin NJ. Preferential potentiation of topoisomerase I poison cytotoxicity by PARP inhibition in S phase. British journal of cancer. 2014;111(7):1319-26.
7. Bajrami I, Frankum JR, Konde A, Miller RE, Rehman FL, Brough R, et al. Genome-wide profiling of genetic synthetic lethality identifies CDK12 as a novel determinant of PARP1/2 inhibitor sensitivity. Cancer research. 2014;74(1):287-97.
8. Johnson SF, Cruz C, Greifenberg AK, Dust S, Stover DG, Chi D, et al. CDK12 Inhibition Reverses De Novo and Acquired PARP Inhibitor Resistance in BRCA Wild-Type and Mutated Models of Triple-Negative Breast Cancer. Cell reports. 2016;17(9):2367-81.
9. Yamamoto TM, McMellen A, Watson ZL, Aguilera J, Ferguson R, Nurmemmedov E, et al. Activation of Wnt signaling promotes olaparib resistant ovarian cancer. Molecular carcinogenesis. 2019.
10. Watson ZL, Yamamoto TM, McMellen A, Kim H, Hughes CJ, Wheeler LJ, et al. Histone methyltransferases EHMT1 and EHMT2 (GLP/G9A) maintain PARP inhibitor resistance in high-grade serous ovarian carcinoma. Clin Epigenetics. 2019;11(1):165.
11. Bitler BG, Watson ZL, Wheeler LJ, Behbakht K. PARP inhibitors: Clinical utility and possibilities of overcoming resistance. Gynecologic oncology. 2017;147(3):695-704.
12. Okonogi TM, Alley SC, Harwood EA, Hopkins PB, Robinson BH. Phosphate backbone neutralization increases duplex DNA flexibility: a model for protein binding. Proceedings of the National Academy of Sciences of the United States of America. 2002;99(7):4156-60.
13. Bannister AJ, Kouzarides T. Regulation of chromatin by histone modifications. Cell Res. 2011;21(3):381-95.
14. Audia JE, Campbell RM. Histone Modifications and Cancer. Cold Spring Harbor perspectives in biology. 2016;8(4):a019521.
15. Esteller M. Cancer epigenomics: DNA methylomes and histone-modification maps. Nature reviews Genetics. 2007;8(4):286-98.
16. Wang R, Xin M, Li Y, Zhang P, Zhang M. The Functions of Histone Modification Enzymes in Cancer. Curr Protein Pept Sci. 2016;17(5):438-45.
17. Lu J, He X, Zhang L, Zhang R, Li W. Acetylation in Tumor Immune Evasion Regulation. Front Pharmacol. 2021;12:771588.
18. Garcia-Ramirez M, Rocchini C, Ausio J. Modulation of chromatin folding by histone acetylation. The Journal of biological chemistry. 1995;270(30):17923-8.

19. Tse C, Sera T, Wolffe AP, Hansen JC. Disruption of higher-order folding by core histone acetylation dramatically enhances transcription of nucleosomal arrays by RNA polymerase III. Molecular and cellular biology. 1998;18(8):4629-38.
20. Duan MR, Smerdon MJ. Histone H3 lysine 14 (H3K14) acetylation facilitates DNA repair in a positioned nucleosome by stabilizing the binding of the chromatin Remodeler RSC (Remodels Structure of Chromatin). The Journal of biological chemistry. 2014;289(12):8353-63.
21. Zhao M, Geng R, Guo X, Yuan R, Zhou X, Zhong Y, et al. PCAF/GCN5-Mediated Acetylation of RPA1 Promotes Nucleotide Excision Repair. Cell reports. 2017;20(9):1997-2009.
22. Ogiwara H, Ui A, Otsuka A, Satoh H, Yokomi I, Nakajima S, et al. Histone acetylation by CBP and p300 at double-strand break sites facilitates SWI/SNF chromatin remodeling and the recruitment of non-homologous end joining factors. Oncogene. 2011;30(18):2135-46.
23. Tamburini BA, Tyler JK. Localized histone acetylation and deacetylation triggered by the homologous recombination pathway of double-strand DNA repair. Molecular and cellular biology. 2005;25(12):4903-13.
24. Ogiwara H, Kohno T. CBP and p300 histone acetyltransferases contribute to homologous recombination by transcriptionally activating the BRCA1 and RAD51 genes. PloS one. 2012;7(12):e52810.
25. Niida H, Matsunuma R, Horiguchi R, Uchida C, Nakazawa Y, Motegi A, et al. Phosphorylated HBO1 at UV irradiated sites is essential for nucleotide excision repair. Nat Commun. 2017;8:16102.
26. Matthews BG, Bowden NA, Wong-Brown MW. Epigenetic Mechanisms and Therapeutic Targets in Chemoresistant High-Grade Serous Ovarian Cancer. Cancers. 2021;13(23).
27. Kuo MH, Brownell JE, Sobel RE, Ranalli TA, Cook RG, Edmondson DG, et al. Transcription-linked acetylation by Gcn5p of histones H3 and H4 at specific lysines. Nature. 1996;383(6597):269-72.
28. Grant PA, Eberharter A, John S, Cook RG, Turner BM, Workman JL. Expanded lysine acetylation specificity of Gcn5 in native complexes. The Journal of biological chemistry. 1999;274(9):5895-900.
29. Schiltz RL, Mizzen CA, Vassilev A, Cook RG, Allis CD, Nakatani Y. Overlapping but distinct patterns of histone acetylation by the human coactivators p300 and PCAF within nucleosomal substrates. The Journal of biological chemistry. 1999;274(3):1189-92.
30. Lee KK, Workman JL. Histone acetyltransferase complexes: one size doesn't fit all. Nature reviews Molecular cell biology. 2007;8(4):284-95.
31. Nagy Z, Tora L. Distinct GCN5/PCAF-containing complexes function as co-activators and are involved in transcription factor and global histone acetylation. Oncogene. 2007;26(37):5341-57.
32. Jin Q, Yu LR, Wang L, Zhang Z, Kasper LH, Lee JE, et al. Distinct roles of GCN5/PCAF-mediated H3K9ac and CBP/p300-mediated H3K18/27ac in nuclear receptor transactivation. The EMBO journal. 2011;30(2):249-62.
33. MacPherson L, Anokye J, Yeung MM, Lam EYN, Chan YC, Weng CF, et al. HBO1 is required for the maintenance of leukaemia stem cells. Nature. 2020;577(7789):266-70.
34. Wu Q, Heidenreich D, Zhou S, Ackloo S, Kramer A, Nakka K, et al. A chemical toolbox for the study of bromodomains and epigenetic signaling. Nat Commun. 2019;10(1):1915.
35. Feng Y, Vlassis A, Roques C, Lalonde ME, González-Aguilera C, Lambert JP, et al. BRPF3-HBO1 regulates replication origin activation and histone H3K14 acetylation. The EMBO journal. 2016;35(2):176-92.
36. Gyorffy B, Lanczky A, Szallasi Z. Implementing an online tool for genome-wide validation of survival-associated biomarkers in ovarian-cancer using microarray data from 1287 patients. Endocrine-related cancer. 2012;19(2):197-208.

37. Tan TZ, Miow QH, Huang RY, Wong MK, Ye J, Lau JA, et al. Functional genomics identifies five distinct molecular subtypes with clinical relevance and pathways for growth control in epithelial ovarian cancer. EMBO Mol Med. 2013;5(7):1051-66.
38. Tan TZ, Miow QH, Miki Y, Noda T, Mori S, Huang RY, et al. Epithelial-mesenchymal transition spectrum quantification and its efficacy in deciphering survival and drug responses of cancer patients. EMBO Mol Med. 2014;6(10):1279-93.
39. Tan TZ, Yang H, Ye J, Low J, Choolani M, Tan DS, et al. CSIOVDB: a microarray gene expression database of epithelial ovarian cancer subtype. Oncotarget. 2015;6(41):43843-52.
40. Mitsopoulos C, Di Micco P, Fernandez EV, Dolciami D, Holt E, Mica IL, et al. canSAR: update to the cancer translational research and drug discovery knowledgebase. Nucleic acids research. 2021;49(D1):D1074-d82.
41. Matulonis UA, Penson RT, Domchek SM, Kaufman B, Shapira-Frommer R, Audeh MW, et al. Olaparib monotherapy in patients with advanced relapsed ovarian cancer and a germline BRCA1/2 mutation: a multistudy analysis of response rates and safety. Ann Oncol. 2016;27(6):1013-9.
42. Maya-Mendoza A, Moudry P, Merchut-Maya JM, Lee M, Strauss R, Bartek J. High speed of fork progression induces DNA replication stress and genomic instability. Nature. 2018;559(7713):279-84.
43. D'Andrea AD. Mechanisms of PARP inhibitor sensitivity and resistance. DNA Repair (Amst). 2018;71:172-6.
44. Jurkowska RZ, Qin S, Kungulovski G, Tempel W, Liu Y, Bashtrykov P, et al. H3K14ac is linked to methylation of H3K9 by the triple Tudor domain of SETDB1. Nat Commun. 2017;8(1):2057.
45. Liu L, Scolnick DM, Trievel RC, Zhang HB, Marmorstein R, Halazonetis TD, et al. p53 sites acetylated in vitro by PCAF and p300 are acetylated in vivo in response to DNA damage. Molecular and cellular biology. 1999;19(2):1202-9.
46. Xiao Y, Li W, Yang H, Pan L, Zhang L, Lu L, et al. HBO1 is a versatile histone acyltransferase critical for promoter histone acylations. Nucleic acids research. 2021;49(14):8037-59.
47. Feng Y, Vlassis A, Roques C, Lalonde ME, Gonzalez-Aguilera C, Lambert JP, et al. BRPF3-HBO1 regulates replication origin activation and histone H3K14 acetylation. The EMBO journal. 2016;35(2):176-92.
48. Bitler BG, Aird KM, Garipov A, Li H, Amatangelo M, Kossenkov AV, et al. Synthetic lethality by targeting EZH2 methyltransferase activity in ARID1A-mutated cancers. Nature medicine. 2015;21(3):231-8.
49. Zheng Y, Thomas PM, Kelleher NL. Measurement of acetylation turnover at distinct lysines in human histones identifies long-lived acetylation sites. Nat Commun. 2013;4:2203.
50. LaFave LM, Beguelin W, Koche R, Teater M, Spitzer B, Chramiec A, et al. Loss of BAP1 function leads to EZH2-dependent transformation. Nature medicine. 2015;21(11):1344-9.
51. Kim D, Langmead B, Salzberg SL. HISAT: a fast spliced aligner with low memory requirements. Nature methods. 2015;12(4):357-60.
52. Tone AA, Virtanen C, Shaw PA, Brown TJ. Decreased progesterone receptor isoform expression in luteal phase fallopian tube epithelium and high-grade serous carcinoma. Endocrine-related cancer. 2011;18(2):221-34.
53. Tone AA, Begley H, Sharma M, Murphy J, Rosen B, Brown TJ, et al. Gene expression profiles of luteal phase fallopian tube epithelium from BRCA mutation carriers resemble high-grade serous carcinoma. Clinical cancer research : an official journal of the American Association for Cancer Research. 2008;14(13):4067-78.